IEEE Access
Multidisciplinary | Rapid Review | Open Access Journal

Received July 30, 2020, accepted August 9, 2020, date of publication August 12, 2020, date of current version August 24, 2020.

Digital Object Identifier 10.1109/ACCESS.2020.3016063

Fractional Order PID Parameter Tuning for Solar Collector System Based on Frequency Domain Analysis

FANWEI MENG[1], SHUAI LIU[1], AIPING PANG[2], AND KAI LIU[1]
[1]School of Control Engineering, Northeastern University at Qinhuangdao, Qinhuangdao 066004, China
[2]School of Electrical Engineering, Guizhou University, Guiyang 550025, China

Corresponding author: Aiping Pang (417524788@qq.com)

This work was supported in part by the Fundamental Research Funds for the Central Universities under Grant N182304010, in part by the Natural Science Foundation of Hebei Province under Grant F2019501012, and in part by the National Natural Science Foundation of China under Grant 61903072.

ABSTRACT The control aim of parabolic distributed solar collector (PDSC) is to make the heat generated follow the expected reference value when the solar radiation varies unevenly. This article proposes a control strategy based on fractional-order PID (FOPID) to achieve control objectives. Four non-linear constraints and an objective function of the controller are proposed based on the frequency domain. Most studies regard the constraint measuring stability as the objective function, while the real difficulty for the control system design should be how to obtain better robustness. Therefore, this article determines five parameters of FOPID by selecting the constraint measuring robustness as the objective function based on Particle swarm optimization (PSO). Besides, three non-parametric statistical tests, including Friedman ranks, Friedman Aligned ranks and Quade ranks, have been adopted to compare PSO with other evolutionary algorithms to demonstrate its advantage. Finally, the superiority of proposed strategy to previous design is demonstrated by the simulation studies on a PDSC in terms of the control performance of step response, static gain variation, time constant variation, high frequency noise and output interference.

INDEX TERMS Fractional order PID controller (FOPID), parabolic distributed solar collector, robustness, particle swarm optimization.

I. INTRODUCTION

A PDSC is a device that uses a parabolic reflector to change the direction of the sunlight entering the lighting port and focus it on the receiver. A PDSC consists of parabolic shaped mirrors which can concentrate the received sunlight in a receiver tube placed in the central line of the collector in order to heat the thermal carrier fluid flowing in it [1], [2]. The control aim of PDSC is to make the heat generated follow the expected reference value when the solar radiation varies unevenly. Standard control strategies fail to provide excellent performance particularly under changing working conditions due to scattered clouds and the uncleanness of the mirrors [3]. Therefore, numerous control techniques have been combined with a feedforward controller, estimation or identification methodologies such as the indirect adaptive control [4], [5], model predictive control [6]–[8], adaptive fuzzy switching control [9] and more advanced adaptive techniques [10], [11].

The classical PID controller is one of the most used controllers in industry for closed-loop control thanks to its simplicity in real time implementation [12], [13]. However, due to the significant variations in the heat transfer process affected by the external disturbances, satisfactory performance covering the total range of disturbances is difficult to reach with a classical PID without an external compensation. Therefore, this article combines fractional calculus with classical PID control [12]–[15]. FOPID controller is a generalization of PID controller considering fractional derivative and integral action. The FOPID controller is proposed by Professor I. Podlubny [15], and is generally simply expressed as $PI^{\lambda}D^{\mu}$. In recent years, fractional calculus has gained significant attention in various applications in engineering and science. Apart from modeling, the fractional calculus has been applied for control design. Compared with classical

The associate editor coordinating the review of this manuscript and approving it for publication was Mingjian Cui.

PID, FOPID control adds two different parameters to be adjusted: integral order and differential order, which makes the setting range of the control parameters larger. Therefore, better robust control effect can be obtained. At present, many studies have explored the characteristics of FOPID and compared its performance with classical PID in different environments [16]–[23].

And various papers have proposed different optimization tuning methods for FOPID: In [17], a method based on solving a set of nonlinear equations is proposed. In [18] and [19], a tuning rule for FOPID controller suitable for motion systems is given. In [20], Genetic algorithm is adopted to design the FOPID controller. Another class of FOPID controller is proposed in [21], which ensures robustness to the closed-loop static gain variation of traditional Crone templates [22]. A multi-objective extremal optimization algorithm is adopted to design FOPID controller for an islanded microgrid [24]. [25] presents a novel FOPID controller design method based on an improved multi-objective extremal optimization algorithm for an automatic regulator voltage system. Besides, there are some effective FOPID tuning settings summarized in [23].

In this article, a linear approximation model of PDSC is established, and a FOPID controller is designed to manage the heat generation based on the model. The five parameters of FOPID are optimized by solving a nonlinear optimization problem based on PSO. Finally, the proposed FOPID model is simulated and compared with the previous FOPID design.

This article is organized as follows: Section II introduces the basics of fractional calculus. In section III, a linear approximation model of a solar collector is established. The design and debugging process of the FOPID controller is described in section IV. The detailed performance analyses are presented between the proposed FOPID and the previous FOPID in section V, and the conclusion is given in the final section.

II. FRACTIONAL CALCULUS

Fractional calculus is a generalization of differential and integral which extends the order from integer to any real number. The fundamental operator is ${}_0\mathbf{D}_t^{\alpha}$, where α is the order and t denotes the limit of the operation. When α is positive, the operator represents fractional differential. While α is negative, the operator represents fractional integral. It can be seen that the fractional calculus operator ${}_0\mathbf{D}_t^{\alpha}$ unifies integration and differentiation [26]. There are numerous definitions of the fractional calculus operator. The most commonly used definitions are the Riemann-Liouville (RL) definition and the Grumwald-Letnikov (GL) definition [16], [23].

In this article, the fractional calculus definition we use is the GL definition:

$$ {}_0\mathbf{D}_t^{\alpha} = \lim_{t\to 0} \frac{1}{\Gamma(\alpha)h^{\alpha}} \sum_{k=0}^{\frac{t-\alpha}{n}} \frac{\Gamma(k+\alpha)}{\Gamma(k+1)} f\left(t-kh\right) \tag{1} $$

where, $n \in N, \alpha \in R^{+}$, Γ is the famous Euler Gamma function.

The most commonly used algebraic tool to describe fractional-order systems is Laplace transform which transforms the system from time domain to frequency domain for analysis and research. When $t = 0$, the Laplace transform of signal $x(t)$ with the differential order of n is:

$$ L\left\{\mathrm{D}^n x(t)\right\} = s^n X(s) \tag{2} $$

Assuming $a_i, b_i \in R, \alpha_i, \beta_i \in R^{+}$ and $\forall i \in N^{*}$, the fractional calculus equation can be defined as follows:

$$ \begin{aligned} &\left(a_n\mathbf{D}^{\alpha_n} + a_{n-1}\mathbf{D}^{\alpha_{n-1}} + \cdots + a_0\right) y(t) \\ &\quad = \left(b_m\mathbf{D}^{\beta_m} + b_{m-1}\mathbf{D}^{\beta_{m-1}} + \cdots + b_0\right) u(t) \end{aligned} \tag{3} $$

Assuming initial conditions are zero, the transfer function of the fractional equation can be obtained as shown in equation (4):

$$ \frac{Y(s)}{U(s)} = \frac{b_m s^{\beta_m} + b_{m-1}s^{\beta_{m-1}} + \cdots + b_0}{a_n s^{\alpha_n} + a_{n-1}s^{\alpha_{n-1}} + \cdots + a_0} \tag{4} $$

III. CONTROL PROBLEM FORMULATION

A PDSC is an industrial system producing thermal energy using heat transfer in thermal carrier fluid. The collector concentrates the received sunlight with its parabolic shaped mirrors to heat the central tube where the fluid flows. Generally, we use the temperature of the fluid to indicate how much heat it contains. The fluid is powered by the system water pump to transfer the thermal energy to the collector via the central tube, and the collector stores energy. The temperature of the fluid flowing out of the collector is reduced and the heat distribution is uneven. We select the temperature of the outgoing fluid as the output signal of the system. The heat distribution of the fluid in the central tube is measured by the heat distribution detector, and it is used as the feedback signal of the control system. The output signal of the controller drives the mirror to rotate a certain angle so that the solar energy is evenly distributed to generate a fluid with uniform heat. Therefore, in this control system, our control objective is to control the angle of the parabolic reflector so that the solar energy obtained can be well distributed. Its device schematic is shown in FIGURE. 1.

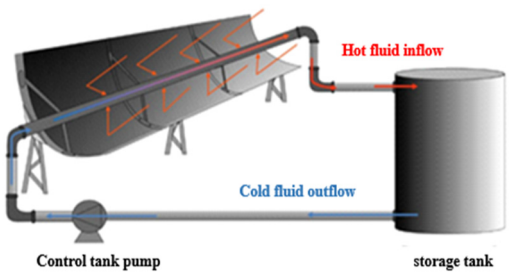

FIGURE 1. Principle diagram of PDSC system.

In order to achieve control purposes, when the disturbance is small, the controlled object can be approximated by the

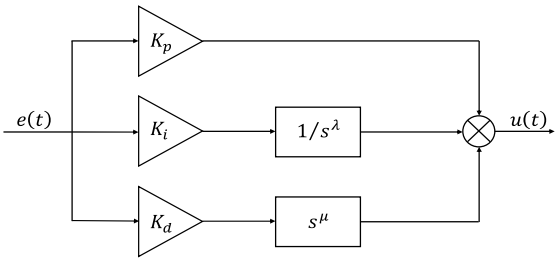

FIGURE 2. The structure diagram of FOPID controller.

following linear system:

$$P(s) = \frac{y(s)}{\bar{u}(s)} = \frac{K}{1+Ts} \tag{5}$$

where s is Laplace operator, $y(s)$ is the Laplace transform of the temperature signal of the outflow fluid, and $\bar{u}(s)$ is the Laplace transform of the input function of the fluid. Meanwhile, the input signal $\bar{u}(t)$ is constrained by the physical limitations of the system:

$$0 < \bar{u}(t)_{min} < \bar{u}(t) < \bar{u}(t)_{max} \tag{6}$$

From the above, the transfer function of the controlled object can be calculated [27]:

$$P(s) = \frac{160.2}{1+6.667s} \tag{7}$$

IV. FOPID CONTROL DESIGN

A. DESIGN PRINCIPLE OF FOPID CONTROLLER

FIGURE 2 is the structure diagram of a FOPID controller. It can be seen from the diagram that the difference between the FOPID controller and the classical PID controller lies in the introduction of two parameters, namely integral order λ and differential order μ. Therefore, the debugging range of FOPID controller is wider and more flexible.

The transfer function of the FOPID controller has the following general form:

$$K(s) = \frac{U(s)}{E(s)} = K_p + \frac{K_i}{s^\lambda} + K_d s^\mu \tag{8}$$

This article proposes a frequency design method of FOPID controller based on nonlinear optimization. The controlled object $P(s)$ and the controller $C(s)$ should satisfy the following frequency domain constraints:

- Crossover frequency and phase margin constraints

Amplitude margin and phase margin have always been considered as important indicators of system stability. Besides, the phase margin is related to the damping of the system. Therefore, it can also be regarded as an index of the response performance of the system. The definitions of phase margin and crossover frequency are shown in equations (9) and (10):

$$\left|G\left(j\omega_{gc}\right)\right|_{\mathrm{dB}} = \left|C\left(j\omega_{gc}\right)P\left(j\omega_{gc}\right)\right|_{\mathrm{dB}} = 0\mathrm{dB} \tag{9}$$

$$\arg\left[G\left(j\omega_{gc}\right)\right] = \arg\left[C\left(j\omega_{gc}\right)P\left(j\omega_{gc}\right)\right] = -\pi + \phi_m \tag{10}$$

- Robust constraint against gain variations

This constraint forces the slope of the phase curve of the open loop system $G(s)$ near the crossover frequency ω_{gc} to be zero. Therefore, the designed controller is robust to gain variations, and the overshoot remains basically unchanged as the system gain changes. The mathematical expression is shown in formula (11).

$$\left(\frac{d}{d\omega}\left(\arg\left[G\left(j\omega\right)\right]\right)\right)_{\omega=\omega_{gc}} = 0 \tag{11}$$

- High frequency noise suppression constraint

The following constraint is proposed for the complementary sensitivity function of the system:

$$\begin{aligned} |T(j\omega)|_{\mathrm{dB}} &= \left|\frac{C(j\omega)P(j\omega)}{1+C(j\omega)P(j\omega)}\right|_{\mathrm{dB}} \le A\mathrm{dB}, \quad \forall\omega \ge \omega_t \\ &\Rightarrow |T(j\omega_t)|_{\mathrm{dB}} = A\mathrm{dB} \end{aligned} \tag{12}$$

where, $A\ dB$ is the amplitude of the complementary sensitivity function required for noise suppression when frequency $\omega \ge \omega_t\ rad/s$.

- Output interference suppression constraint

The following constraint is presented for the sensitivity function of the system:

$$\begin{aligned} |S(j\omega)|_{\mathrm{dB}} &= \left|\frac{1}{1+C(j\omega)P(j\omega)}\right|_{\mathrm{dB}} \le B\mathrm{dB}, \quad \forall\omega \le \omega_s \\ &\Rightarrow |S(j\omega_s)|_{\mathrm{dB}} = B\mathrm{dB} \end{aligned} \tag{13}$$

where, $B\ dB$ is the amplitude of the sensitivity function required for output interference suppression when the frequency $\omega \le \omega_s rad/s$.

- Elimination of static errors

The steady state error of the closed-loop system can be automatically eliminated by the introduction of fractional integration.

B. PARAMETER DEBUGGING OF FOPID CONTROLLER

The previous section introduces the design principle of the FOPID controller based on the frequency domain. Five nonlinear constraints (9) $\sim$ (13) are proposed to solve the five unknown parameters ($K_p, K_i, K_d, \lambda, \mu$) of the FOPID controller C (s). Using FMINCON function for nonlinear optimization needs to solve the selection of the objective function and the determination of the initial value. Most studies (such as [27]) treat the above equation (9) as the objective function and the other four as constraints. This design only considers the stability of control system. However, the real difficulty for the controller design should be how to make the system obtain better robustness. Besides, the selection of the initial value also determines whether the FMINCON function can obtain a desired optimal solution. However, the determination of the initial value in existing designs mostly depends on experience and attempts.

Considering the above two weaknesses, we have made following improvements: Firstly, select the equation (11) measuring robustness as the objective function and other four

conditions as constraints. Secondly, PSO is adopted to obtain the global optimal solution.

First, compile the fitness function. As can be seen from the above, the equation (11) is used as the objective function. The fitness function can be obtained as follows:

$$Fit[f(\omega)] = \left(\frac{d}{d\omega}\left(\arg\left[G\left(j\omega\right)\right]\right)\right)_{\omega=\omega_{gc}} \tag{14}$$

In order to facilitate compiling programs in MATLAB, we need to transform the functions to the following forms:

- The transfer function of the first-order system:

$$P\left(j\omega\right) = \frac{K}{jT\omega+1} = \frac{K}{1+\omega^2T^2} + j\cdot\frac{-KT\omega}{1+\omega^2T^2} \tag{15}$$

- The transfer function of FOPID controller:

$$C\left(j\omega\right) = K_p + \frac{K_i}{(j\omega)^{\lambda}} + K_d\cdot(j\omega)^{\mu} = r + j\cdot s \tag{16}$$

where, r is the real part and s is the imaginary part. According to De Moivre's theorem:

$$[r\cdot(\cos\theta + i\cdot\sin\theta)]^n = r^n\cdot(\cos n\theta + i\cdot\sin n\theta) \tag{17}$$

Therefore:

$$\begin{aligned}(j\omega)^{\lambda} &= [\omega\cdot(\cos\frac{\pi}{2} + i\cdot\sin\frac{\pi}{2})]^{\lambda}\\ &= \omega^{\lambda}\cdot(\cos\frac{\pi\lambda}{2} + i\cdot\sin\frac{\pi\lambda}{2})\\ (j\omega)^{\mu} &= [\omega\cdot(\cos\frac{\pi}{2} + i\cdot\sin\frac{\pi}{2})]^{\mu}\\ &= \omega^{\mu}\cdot(\cos\frac{\pi\mu}{2} + i\cdot\sin\frac{\pi\mu}{2})\end{aligned} \tag{18}$$

Bring it into $C\left(j\omega\right)$:

$$\begin{aligned}r &= K_p + K_i\cdot\omega^{-\lambda}\cdot\cos(\frac{-\lambda\pi}{2}) + K_d\cdot\cos(\frac{-\lambda\pi}{2})\\ s &= K_p + K_i\cdot\omega^{-\lambda}\cdot\sin(\frac{-\lambda\pi}{2}) + K_d\cdot\sin(\frac{-\lambda\pi}{2})\end{aligned} \tag{19}$$

- Amplitude $\left|G\left(j\omega_{gc}\right)\right|$ of the open-loop system:

$$\begin{aligned}\left|G\left(j\omega_{gc}\right)\right| &= \left|C\left(j\omega_{gc}\right)P\left(j\omega_{gc}\right)\right|\\ &= \left|C\left(j\omega_{gc}\right)\right|\cdot\left|P\left(j\omega_{gc}\right)\right|\\ &= \sqrt{r^2+s^2}\cdot\left[K\Big/\sqrt{\omega_{gc}^2\cdot T^2+1}\right]\end{aligned} \tag{20}$$

- Phase angle of the open-loop system:

$$\begin{aligned}\arg\left[G\left(j\omega_{gc}\right)\right] &= \arg\left[C\left(j\omega_{gc}\right)P\left(j\omega_{gc}\right)\right]\\ &= \arg\left[C\left(j\omega_{gc}\right)\right] + \arg\left[P\left(j\omega_{gc}\right)\right]\\ &= \arctan(s_{gc}/r_{gc}) + \arctan(-1/\omega_{gc}T)\end{aligned} \tag{21}$$

- Robustness constraint for gain variations:

$$\left(\frac{d}{d\omega}\left(\arg\left[G\left(j\omega\right)\right]\right)\right)_{\omega=\omega_{gc}} = 0$$

$$\begin{aligned}&\left(\frac{d}{d\omega}\left(\arg\left[G\left(j\omega\right)\right]\right)\right)_{\omega=\omega_{gc}}\\ &= \frac{d}{d\omega}\left[\arctan(s_{gc}/r_{gc})\right] + \frac{d}{d\omega}\left[\arctan(-1/\omega_{gc}T)\right]\\ &= \frac{1}{1+(s_{gc}/r_{gc})^2}\cdot\left[\frac{s'_{gc}r_{gc}-r'_{gc}s_{gc}}{r_{gc}^2}\right] + \frac{T}{1+(T\omega_{gc})^2}\end{aligned} \tag{22}$$

- The high frequency noise suppression constraint:

$$\begin{aligned}\left|T\left(j\omega\right)\right| &= \left|\frac{C\left(j\omega\right)P\left(j\omega\right)}{1+C\left(j\omega\right)P\left(j\omega\right)}\right|\\ &= \frac{\left|C\left(j\omega\right)\right|}{\left|1/P\left(j\omega\right)+C\left(j\omega\right)\right|}\\ &= \mathrm{K}\cdot\frac{\sqrt{r^2+s^2}}{\sqrt{(1+K\cdot r)^2+(T\omega+K\cdot s)^2}}\end{aligned} \tag{23}$$

- Output interference suppression constraint:

$$\begin{aligned}\left|S\left(j\omega\right)\right| &= \left|\frac{1}{1+C\left(j\omega\right)P\left(j\omega\right)}\right|\\ &= \frac{\left|1/P\left(j\omega\right)\right|}{\left|1/P\left(j\omega\right)+C\left(j\omega\right)\right|}\\ &= \frac{\sqrt{(\omega T)^2+1}}{\sqrt{(1+K\cdot r)^2+(T\omega+K\cdot s)^2}}\end{aligned} \tag{24}$$

After analyzing the above constraints in the frequency domain, as long as we substitute the parameter values set by each constraint, we can debug and solve five parameters through PSO. FIGURE 3 shows the flowchart of PSO.

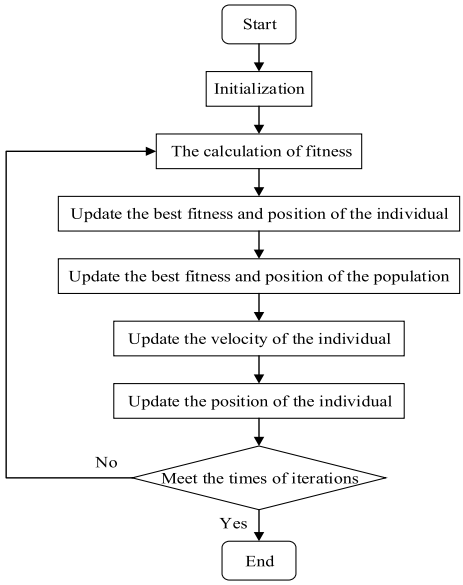

FIGURE 3. The flowchart of PSO.

PSO is essentially a stochastic algorithm. In order to demonstrate the superiority of PSO to other evolutionary algorithms, we execute a number of comparisons between PSO and other evolutionary algorithms, such as Differential Evolution (DE), Genetic Algorithm (GA) and Genetic Algorithm-FMINCON (GA-F). The specific parameter settings of different evolutionary algorithms are proposed in TABLE 1.

TABLE 1. The parameter settings of different evolutionary algorithms.

Evolutionary algorithms	Parameter settings
Differential Evolution (DE)	Population size = 50 The times of iterations = 100 The coefficient of variation = 0.4 Crossover probability = 0.1
Genetic Algorithm (GA)	Population size = 50 The times of iterations = 100 Crossover probability = 0.8 Mutation probability = 0.1
Genetic Algorithm-FMINCON (GA-F)	Population size = 50 The times of iterations = 100 Crossover probability = 0.8 Mutation probability = 0.1 'TolX' = 1e-10 'TolFun' = 1e-10 'TolCon' = 1e-10 'MaxFunEval' = 100000 'DiffMinChange' = 1e-10 'Algorithm' = 'sqp'
Particle Swarm Optimization (PSO)	Population size = 50 The times of iterations = 100 The weight of inertia = 0.8 The self-learning factor = 0.5 The population-learning factor=0.5 The speed boundary = [-1.5,1.5]

TABLE 2. Statistical results of different algorithms.

	$F_{\max}$	$F_{\min}$	F_{ave}	F_{std}	$Time(s)$
DE	0.8925	0.0918	0.4283	0.2139	0.1336
GA	1.0366	0.1322	0.4576	0.2572	1.9267
GA-F	0.2452	0.0591	0.0777	0.0558	1.9781
PSO	0.7960	0.0236	0.1075	0.1514	0.0946

Each algorithm is implemented independently for 30 times. TABLE 2 presents the statistical results of each algorithm including the maximum, average, minimum, standard deviation values of the objective function, and the average computational time. According to TABLE 2, we can see that PSO has an evident advantage of minimum and average computational time over other algorithms.

Furthermore, according to the research works with respect to the non-parametric statistical tests for different algorithms [28], [29], some statistical tests have been adopted to compare the performance of DE, GA, GA-F and PSO. TABLE 3 proposes ranks achieved by Friedman, Friedman aligned and Quade tests for the objective function obtained by different algorithms. It is noticeable from TABLE 3 that PSO performs best in all statistical tests. Consequently, PSO has the superiority over other evolutionary algorithms in solving five parameters of FOPID.

TABLE 3. The ranks achieved by Friedman, Friedman aligned and Quade tests.

	Friedman ranks	Friedman Aligned ranks	Quade ranks
DE	2.8	10.8	2.67
GA	3.8	16.2	3.67
GA-F	1.8	8.4	2.07
PSO	1.6	6.6	1.60

V. NUMERICAL SIMULATIONS

The parameters of the frequency domain constraints proposed in this article for the solar collector system are as follows:

- Crossover frequency constraint:

$$\omega_{gc} = 1\text{rad}/\text{s} \tag{25}$$

- Phase margin constraint:

$$\phi_m = 65^\circ \tag{26}$$

- Robust constraint against gain variations:

$$\left(\frac{d}{d\omega}(\arg[G(j\omega)])\right)_{\omega=\omega_{gc}} = 0 \tag{27}$$

- Noise suppression constraint:

$$\forall\omega \le \omega_s = 0.01\text{rad}/\text{s}, \quad |T(j\omega)|_{\text{dB}} \le -10\text{dB} \tag{28}$$

- Output interference suppression constraint:

$$\forall\omega \ge \omega_t = 10\text{rad}/\text{s}, \quad |S(j\omega)|_{\text{dB}} \le -20\text{dB} \tag{29}$$

The upper and lower limits of the parameters of controllers are as follows:

$$0.01 \le K_p \le 10, \quad 0.01 \le K_i \le 10, \ 0.01 \le K_d \le 10$$
$$0.1 \le \lambda \le 1, \quad 0.1 \le \mu \le 1.$$

The FOPID1 and FOPID2 controllers are obtained by using Equation (11) and Equation (9) as objective functions respectively. Specific parameters are presented in TABLE 4.

TABLE 4. The parameters of different controllers.

Controller type	Kp	Ki	Kd	λ	μ
FOPID1	0.01	0.0327	0.01	0.6012	0.1
FOPID2	0.0126	0.0366	0.01	0.67	0.6973

A. THE ANALYSIS OF STEP RESPONSE PERFORMANCE

In this section, we execute the analysis of step response performance of the two controllers. The comparison of dynamic response of the closed-loop system is shown in FIGURE 5. Specific performance indexes can refer to TABLE 5. It can be seen that the rise time, peak time, steady state time and overshoot of the former are less than those of the latter.

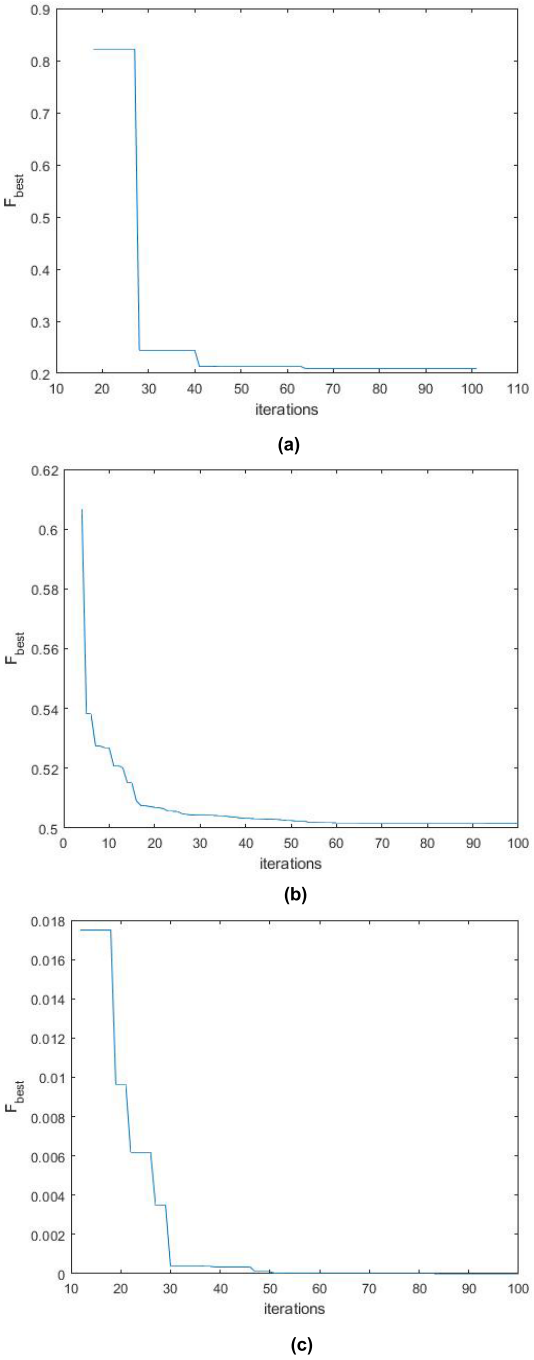

FIGURE 4. Convergence graphs of the optimization algorithms. (a) DE (b) GA (c) PSO.

Therefore, the response performance of FOPID1 is better than that of FOPID2.

In addition, the comparative performance evaluation has been also studied in the frequency domain. The bode diagram of the open-loop system is shown in FIGURE 6, and it is noticeable from the diagram that the two controllers fully satisfy the design constraints (25) and (26). However, the phase margin of FOPID1 stays relatively more stable than that of FOPID2 near the crossover frequency.

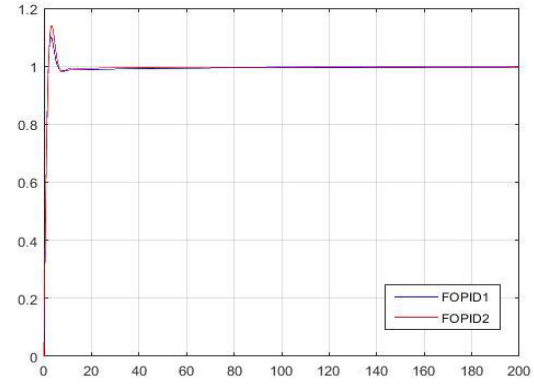

FIGURE 5. The comparison of step response curves.

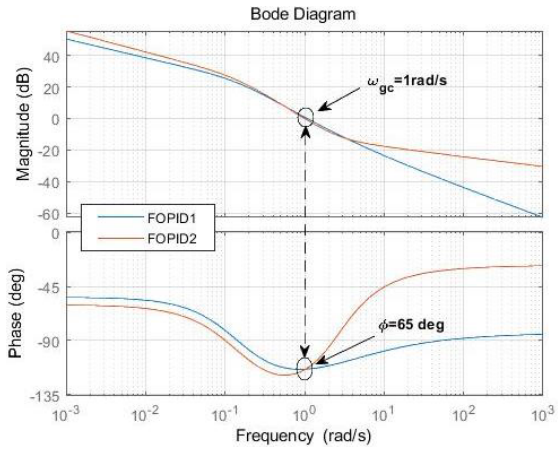

FIGURE 6. The bode diagram of open-loop systems.

TABLE 5. The performance indexes of step curves.

Controller type	Rise time	Peak time	Steady state time	Overshoot
FOPID1	1.88	2.99	5.16	10.3%
FOPID2	1.94	3.24	5.67	14.2%

B. THE ROBUSTNESS ANALYSIS OF SYSTEM GAIN AND LOAD VARIATION

The robustness analysis of system gain and load variation is conducted in this section. The dynamic response curves of FOPID1 and FOPID2 are shown in FIGURE 7 and FIGURE 8 respectively when the system static gain varies $\pm 10\%$ and the input reference value changes in the 100s. As is shown in the figures, FOPID1 performs better than the other. The overshoot of former is significantly less than the latter.

Moreover, TABLE 6 presents more specific performance metrics. The above table shows that the changes of performance metrics of FOPID1 are less than those of FOPID2. Therefore, the former is more robust than the latter.

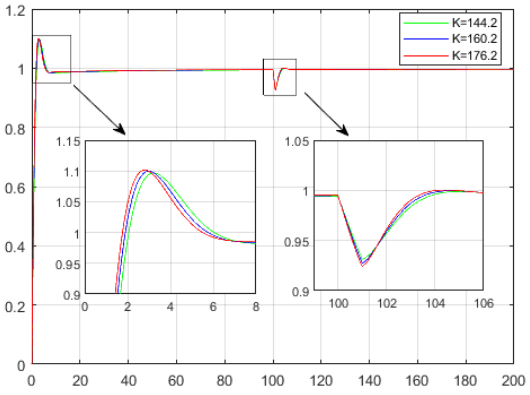

FIGURE 7. Step response curves of FOPID1 controller for different gain and load variation.

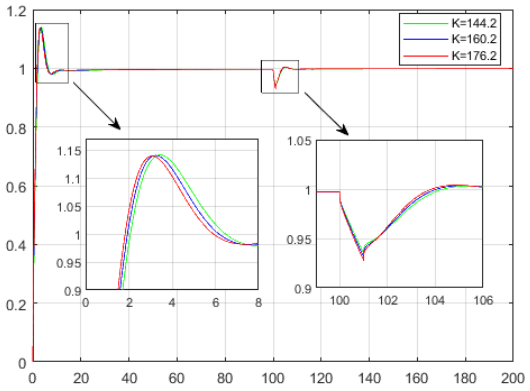

FIGURE 8. Step response curves of FOPID2 controller for different gain and load variation.

TABLE 6. Performance metrics of system response under different gain.

Gain variation	Controller type	Rise time	Peak time	Steady state time	overshoot
K=144.2	FOPID1	2.04	3.22	5.46	10.1%
	FOPID2	2.07	3.44	5.98	14.3%
K=160.2	FOPID1	1.88	2.99	5.16	10.3%
	FOPID2	1.94	3.24	5.67	14.2%
K=176.2	FOPID1	1.75	2.8	4.89	10.5%
	FOPID2	1.83	3.07	5.42	14.1%

C. THE ROBUSTNESS ANALYSIS OF SYSTEM TIME CONSTANT VARIATION

This section provides the robustness analysis of system time constant variation. FIGURE 9 and FIGURE 10 provide the step curves of FOPID1 and FOPID2 respectively when system time constant changes ±20%. More specific metrics can refer to the data in the TABLE 7. It is demonstrated by the above table that FOPID1 has better response performance than the other. This means that FOPID1 is more robust to time constant variation.

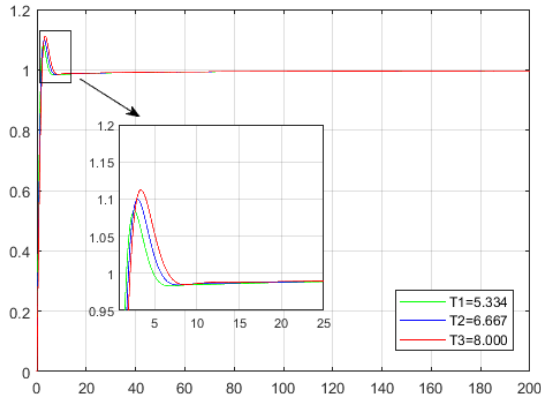

FIGURE 9. Step response curves of FOPID1 controller for different time constant.

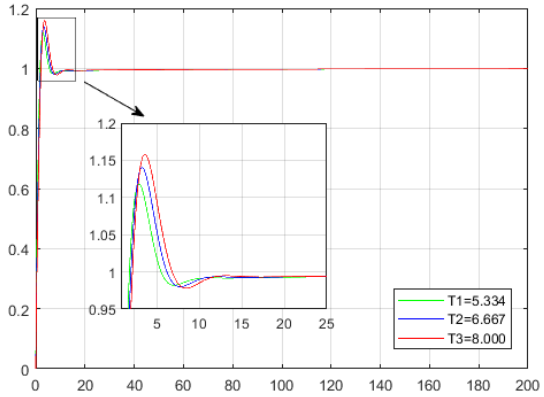

FIGURE 10. Step response curves of FOPID2 controller for different time constant.

TABLE 7. Performance metrics of system response under different time constant.

Time variation	Controller type	Rise time	Peak time	Steady state time	Overshoot
T=5.334	FOPID1	1.66	2.58	4.31	8.8%
	FOPID2	1.75	2.89	4.98	12.0%
T=6.667	FOPID1	1.88	2.99	5.16	10.3%
	FOPID2	1.94	3.24	5.67	14.2%
T=8.000	FOPID1	2.1	3.38	5.93	11.6%
	FOPID2	2.11	3.57	8.67	16.0%

D. THE ROBUSTNESS ANALYSIS OF HIGH FREQUENCY NOISE AND OUTPUT INTERFERRENCE

In order to make the system more robust to noise and output interference, we propose noise suppression constraint (28) and output interference suppression constraint (29). The comparisons of the bode diagrams of the sensitivity function and complementary sensitivity function are shown in FIGURE 11 and FIGURE 12 respectively.

These two controllers both satisfy the constraint (28) in FIGURE 11. However, as can be seen in FIGURE 12, FOPID2 dissatisfies the interference suppression constraint (29) while FOPID1 satisfies. Besides, FOPID1 has greater

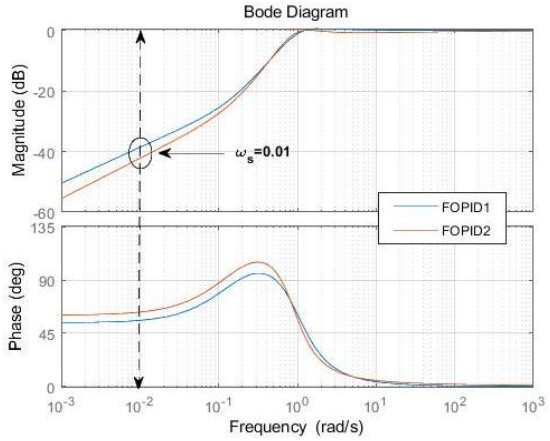

FIGURE 11. The bode diagram of sensitivity function (output interference suppression).

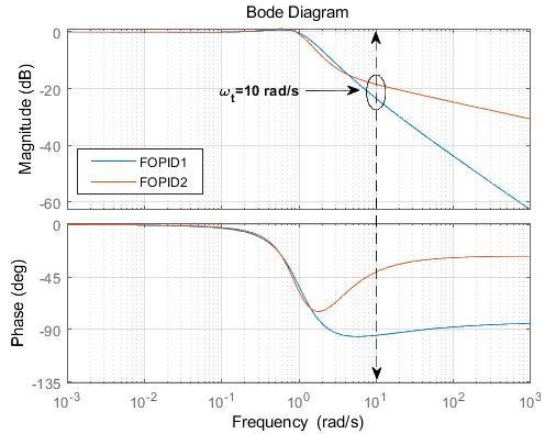

FIGURE 12. The bode diagram of the complementary sensitivity function (noise suppression).

frequency attenuation in the high frequency domain, which means that FOPID1 obtains a stronger high-frequency noise suppression ability.

VI. CONCLUSION

In this article, an improved FOPID control strategy by constrained nonlinear optimization has been proposed to control the PDSC. PSO has been adopted to determine the five parameters of FOPID controller. Moreover, three non-parametric statistical tests, including Friedman ranks, Friedman Aligned ranks and Quade ranks, have been employed to compare PSO with other evolutionary algorithms to demonstrate its advantage. Finally, through the simulation results, the proposed FOPID has better control characteristics and robustness in comparison with previous FOPID design.

REFERENCES

[1] M. E. Gi, M. Li, and Y. F. Wang, "Numerical simulation and optimization of parabolic trough cativy solar collector system," *Acta Energiae Solaris Sinica*, vol. 39, no. 11, pp. 3060–3068, 2018.
[2] X. Han, Z. M. Wang, and R. Tian, "Numerical simulation of thermal efficiency on trough solar collector," *Acta Energiae Solaris Sinica*, vol. 37, no. 9, pp. 2265–2270., 2016
[3] E. F. Camacho, F. R. Rubio, M. Berenguel, and L. Valenzuela, "A survey on control schemes for distributed solar collector fields. Part I: Modeling and basic control approaches," *Sol. Energy*, vol. 81, no. 10, pp. 1240–1251, 2007.
[4] F. P. Yu, X. Zhang, and G. H. Wang, "Research on controller of PWM constant current based on adaptive PI control for photovoltaic LED lighting systems," *ACTA Energiae Solaris Sinica*, vol. 27, no. 2, pp. 132–135, 2006.
[5] J. M. Igreja, J. M. Lemos, and R. N. Silva, "Adaptive receding horizon control of a distributed collector solar field," in *Proc. 44th IEEE Conf. Decis. Control*, Dec. 2005, pp. 1282–1287.
[6] E. F. Camacho and M. Berenguel, "Robust adaptive model predictive control of a solar plant with bounded uncertainties," *Int. J. Adapt. Control Signal Process.*, vol. 11, no. 4, pp. 311–325, 1997.
[7] M. Gálvez-Carrillo, R. De Keyser, and C. Ionescu, "Nonlinear predictive control with dead-time compensator: Application to a solar power plant," *Sol. Energy*, vol. 83, no. 5, pp. 743–752, May 2009.
[8] A. J. Gallego and E. F. Camacho, "Adaptative state-space model predictive control of a parabolic-trough field," *Control Eng. Pract.*, vol. 20, no. 9, pp. 904–911, 2012.
[9] J. Henriques, A. Cardoso, and A. Dourado, "Supervision and c-Means clustering of PID controllers for a solar power plant," *Int. J. Approx. Reasoning*, vol. 11, pp. 311–325, Sep./Oct. 1999.
[10] G. Pin, M. Falchetta, and G. Fenu, "Adaptive time-warped control of molten salt distributed collector solar fields," *Control Eng. Pract.*, vol. 16, pp. 813–823, Jul. 2008.
[11] R. N. Silva, J. M. Lemos, and L. M. Rato, "Variable sampling adaptive control of a distributed collector solar field," *IEEE Trans. Control Syst. Technol.*, vol. 11, no. 5, pp. 765–772, Sep. 2003.
[12] K. J. Åström and T. Hägglund, "The future of PID control," *Control Eng. Pract.*, vol. 9, no. 11, pp. 1163–1175, Nov. 2001.
[13] K. Åström, T. Hagglund, C. C. Hang, and W. K. Ho, "Automatic tuning and adaptation for PID controllers-a survey," *Control Eng. Pract.*, vol. 9, no. 4, pp. 699–714, 1993.
[14] A. J. Gallego and E. F. Camacho, "Estimation of effective solar irradiation using an unscented Kalman filter in a parabolic-trough field," *Sol. Energy*, vol. 86, no. 12, pp. 3512–3518, Dec. 2012.
[15] I. Podlubny, "Fractional-order systems and PI$^{\lambda}\mu$-controllers," *IEEE Trans. Autom. Control*, vol. 44, no. 1, pp. 208–214, Jan. 1999.
[16] I. Podlubny, *Fractional Differential Equations*. New York, NY, USA: Academic, 1999.
[17] C. A. Monje, B. M. Vinagre, V. Feliu, and Y. Chen, "Tuning and auto-tuning of fractional order controllers for industry applications," *Control Eng. Pract.*, vol. 16, no. 7, pp. 798–812, Jul. 2008.
[18] H. Li, Y. Luo, and Y. Chen, "A fractional order proportional and derivative (FOPD) motion controller: Tuning rule and experiments," *IEEE Trans. Control Syst. Technol.*, vol. 18, no. 2, pp. 516–520, Mar. 2010.
[19] J.-G. Lu and G. Chen, "Robust stability and stabilization of fractional-order interval systems: An LMI approach," *IEEE Trans. Autom. Control*, vol. 54, no. 6, pp. 1294–1299, Jun. 2009.
[20] H. Li, Y. Luo, and Y. Chen, "An output feedback approach to the design of robust fractional PI and PID controllers," *Int. J. Soft Comput. Eng.*, no. 3, 2011.
[21] M. Tenoutit, N. Maamri, and J. Trigeassou, "An output feedback approach to the design of robust fractional PI and PID controllers," in *Proc. World Congr. (IFAC)*, Milan, Italy, 2011.
[22] A. Oustaloup, *La Commande CRONE*. Paris, France: Hermes, 1991.
[23] C. A. Monje, Y. Q. Chen, B. M. Vinagre, D. Xue, and V. Feliu, *Fractional-order systems and controls: Fundamentals and Applications*. Berlin, Germany: Springer, 2010.
[24] H. Wang, G. Q. Zeng, Y. X. Dai, D. Bi, J. Sun, and X. Xie, "Design of a fractional order frequency PID controller for an islanded microgrid: A multi-objective extremal optimization method," *Energies*, vol. 10, no. 10, p. 1502, 2017.
[25] G.-Q. Zeng, J. Chen, Y.-X. Dai, L.-M. Li, C.-W. Zheng, and M.-R. Chen, "Design of fractional order PID controller for automatic regulator voltage system based on multi-objective extremal optimization," *Neurocomputing*, vol. 160, pp. 173–184, Jul. 2015.
[26] J.-Y. Cao, J. Liang, and B.-G. Cao, "Optimization of fractional order PID controllers based on genetic algorithms," in *Proc. Int. Conf. Mach. Learn. Cybern.*, 2005, pp. 5686–5689.
[27] S. Elmetennani, I. N'Doye, K. N. Salama, and T.-M. Laleg-Kirati, "Performance analysis of fractional-order PID controller for a parabolic distributed solar collector," in *Proc. IEEE AFRICON*, Cap Town, South Africa, Sep. 2017, pp. 461–466.

[28] J. Derrac, S. García, D. Molina, and F. Herrera, "A practical tutorial on the use of nonparametric statistical tests as a methodology for comparing evolutionary and swarm intelligence algorithms," *Swarm Evol. Comput.*, vol. 1, no. 1, pp. 3–18, Mar. 2011.
[29] G.-Q. Zeng, X.-Q. Xie, M.-R. Chen, and J. Weng, "Adaptive population extremal optimization-based PID neural network for multivariable nonlinear control systems," *Swarm Evol. Comput.*, vol. 44, pp. 320–334, Feb. 2019.

FANWEI MENG received the B.S. degree in automation specialty from Harbin Engineering University, Harbin, China, in 2005, and the Ph.D. degree in control science and engineering from the Harbin Institute of Technology, Harbin, in 2013. From 2005 to 2013, he was a Naval Technical Officer. Since 2014, he has been a Lecturer with the Control Science and Engineering Department, Northeastern University at Qinhuangdao, China. He is the author of one book and more than 20 articles. His research interests include robust control and control system design.

SHUAI LIU is currently pursuing the bachelor's degree with Northeastern University at Qinhuangdao, Qinhuangdao, Hebei, China. He works with Fanwei Meng as a Student Researcher. His current research interest includes automatic control.

AIPING PANG received the M.S. degree from the Mathematics College of Science, Harbin Institute of Technology, China, in 2013, and the Ph.D. degree in control science and engineering from the College of Aerospace, Harbin Institute of Technology, in 2018. She currently works with the Department of Automation, School of Electrical Engineering, Guizhou University, Guiyang, China. Her major research interests include robot control, H-infinity control, delay system control, spacecraft control, and so on.

KAI LIU is currently pursuing the master's degree with Northeastern University at Qinhuangdao, Qinhuangdao, Hebei, China. He works with Fanwei Meng as a Student Researcher. His current research interest includes automatic control.